

PAPER • OPEN ACCESS

## Alumina-based composites reinforced with single-walled carbon nanotubes

To cite this article: A A Leonov and E V Abdulmenova 2019 *IOP Conf. Ser.: Mater. Sci. Eng.* **511** 012001

View the [article online](#) for updates and enhancements.

# Alumina-based composites reinforced with single-walled carbon nanotubes

A A Leonov and E V Abdulmenova

National Research Tomsk Polytechnic University, 30 Lenin Ave., Tomsk, 634050, Russia

Email: laa91@tpu.ru

**Abstract.** Monolithic  $\text{Al}_2\text{O}_3$  ceramics and  $\text{Al}_2\text{O}_3 - 3 \text{ vol\%}$  single-walled carbon nanotubes (SWCNTs) composites were prepared by spark plasma sintering. The influence of SWCNTs and sintering temperature on sintering behavior and mechanical properties were investigated. Nanotubes were relatively homogeneously distributed in the composite powder, although some agglomerates/bundles existed. It was found that SWCNTs addition retards slightly the sinterability of alumina by nanotubes hindering of particle rearrangement. The average microhardness of the composites was lower than that of  $\text{Al}_2\text{O}_3$  ceramics, but there were also high microhardness values of composites (20.41 GPa). The reduction in microhardness is explained in this paper. The average values of the fracture toughness ( $4.94 \text{ MPa}\cdot\text{m}^{1/2}$ ) from the composite sintered at  $1500^\circ\text{C}$  were approximately 6 % and 12 % higher than those from the  $\text{Al}_2\text{O}_3$  ceramics sintered at  $1500^\circ\text{C}$  and  $1600^\circ\text{C}$ , respectively. In addition, the analysis of the phase composition and the parameters of the crystal structure of the samples were made.

## 1. Introduction

Alumina ( $\text{Al}_2\text{O}_3$ ) ceramics possess wide technological applications in modern industry because of their excellent properties such as high hardness, optimal high temperature property retention, acceptable dielectric properties, chemical inertness, corrosion resistance, adsorption properties and biocompatibility. Brittleness, low fracture toughness and flexural strength of alumina ceramics largely limits their application scope [1]. Many strategies have been proposed to tackle this problem and adding reinforcing materials as a second phase in the form of particles, platelets or whiskers/fibers is a useful method [2, 3]. The improvement in toughness with fiber reinforcement, especially in a continuous form, is much greater than that with particulate reinforcement [4]. Reinforcement of the  $\text{Al}_2\text{O}_3$  matrix can be performed different fibrous fillers such as: alumina nanofibers/whiskers [5-8], mullite whiskers [9, 10], SiC whiskers [11, 12], carbon nanofibers [13, 14], carbon nanotubes [15-18], boron nitride nanotubes [19, 20]. Most of investigations have been focused especially on the mechanical characteristics of carbon nanotubes (CNTs) since CNTs with a tubular structure exhibit almost 5 times of elastic modulus and nearly 100 times tensile strength compared to high strength steels. Therefore, it is expected that CNTs can upgrade the mechanical properties of  $\text{Al}_2\text{O}_3$  and make it suitable for numerous advanced applications. For example, Zhan et al. [21] reported a fracture toughness of  $9.7 \text{ MPa}\cdot\text{m}^{1/2}$  in 10 vol% single-walled carbon nanotubes manufactured by spark plasma sintering (SPS) technique versus only  $3.7 \text{ MPa}\cdot\text{m}^{1/2}$  for the matrix, in alumina composites. Bi et al. fabricated fully dense composites of multi-walled carbon nanotubes (MWCNTs) with alumina matrix by using hydrothermal crystallization methods and followed by hot-pressing. The bending strength



and fracture toughness of the sample were increased by 24.6 % and 80.3 % respectively compared with monolithic alumina [22]. Bocanegra-Bernal et al. [23] reported that for 0.1 wt% MWCNT/ $\text{Al}_2\text{O}_3$  composites, the fracture toughness had an increase of 63 % compared with the monolithic alumina. Wang et al. [20] claimed that the alumina grain growth was remarkably inhibited by boron nitride nanotubes (BNNTs), and the fracture toughness and bending strength were increased by 31 % and 67 % for the composites containing 1.0 and 2.0 wt% of BNNTs, respectively. Given that the incorporation of SWCNTs may provide more potential for strengthening and toughening, the effect of SWCNTs content on the mechanical properties of  $\text{Al}_2\text{O}_3$ -based ceramics was investigated in this paper. Spark plasma sintering was employed to obtain  $\text{Al}_2\text{O}_3$ -SWCNTs composites, and the effect of sintering temperatures was also investigated.

## 2. Materials and methods

In the present work, alumina powder with the addition of nanopowder of the same composition in the amount of 6 % was used as the matrix base. Commercial SWCNTs «Tuball» were purchased from OCSiAl, Russia (content of SWCNTs ~ 75 wt%, diameter 1–3 nm and length 1–5  $\mu\text{m}$ ). The SWCNTs was dispersed in ethanol by means of ultrasonic treatment during 5 min and a drop of the suspension was transferred onto a copper grid and by means of transmission electron microscope JEM-2100F (JEOL) its morphology was studied. The measurements of particle size distribution of initial  $\text{Al}_2\text{O}_3$  powder by means of laser diffraction method were performed with SALD-7101 (Shimadzu). The specific surface area of the  $\text{Al}_2\text{O}_3$  powder, SWCNTs and  $\text{Al}_2\text{O}_3$ -SWCNTs composite powder was measured by BET technique using installation Sorbi-M (META). Before mixing, the SWCNTs were first dispersed in ethanol for 30 min by ultrasonic bath (110 W, 35 kHz) to obtain homogeneous ethanol-SWCNTs suspension. Next, an alumina was added to this suspension at the ratio of the SWCNTs 3 vol% and then ultrasonic dispersion was continued for an additional 30 min. After the expiration of the ultrasonic dispersion, the processed composite suspension was put on a magnetic stirrer and agitation was performed for 30 min. After mixing, the slurry was dried at 120 °C for 3 h. The morphology and detailed structure of composite powder were observed by scanning electron microscope JSM-7500FA (JEOL). The resulting powder mixture was placed into a graphite die with an inner diameter of 14 mm and then spark plasma sintered at 1500 °C and 1600 °C respectively for 10 min under a uniaxial load of 40 MPa in vacuum. A heating rate of 100 °C/min was employed. For comparison, monolithic  $\text{Al}_2\text{O}_3$  ceramics were sintered under the same conditions. The bulk density of the sintered samples was measured using the Archimedes method with distilled water as the immersing medium. The relative density was calculated by dividing the bulk density by the theoretical density. Vickers indentation tests were carried out to evaluate the microhardness ( $H_v$ ) and fracture toughness ( $K_{IC}$ ) of sintered  $\text{Al}_2\text{O}_3$  and composites at room temperature. Tests were performed on sample surfaces using a Vickers indenter with a load 4.9 H (PMT-3M, LOMO). The fracture toughness was calculated by using the equation given by Anstis [24]. Analysis of the phase composition and the parameters of the crystal structure of the samples were determined by X-ray diffraction (XRD) equipment diffractometer of XRD-7000S (Shimadzu) type using Cu-K $\alpha$  radiations ( $\lambda = 1.54056 \text{ \AA}$ ). The tube voltage and current were 40 kV and 30 mA respectively. Scan range and sampling pitch were 10 ° – 120 ° and 0.03 °, respectively. XRD data were used to calculate size of the coherently diffracting domain (CDD).

## 3. Results and discussion

Figure 1a shows the TEM-image of the SWCNTs. It is seen that nanotubes are bundles of various widths with sphere-shaped catalyst particles on them or agglomerates of the catalyst particles, which are also sphere-shaped. A large number of bundles have a cross-sectional dimension of 10-40 nm. However, there are even larger bundles up to 200 nm. The bundles of SWCNTs have a flattened ribbonlike shape. Individual nanotubes occur in the images very rarely. Owing to its nanometric diameter, a SWCNT has a very large specific surface area 546.45 m<sup>2</sup>/g [25]. The SEM image of composite powder containing 3 vol% of SWCNTs is shown in Figure 1b. Disentangled SWCNTs are

well dispersed among  $\text{Al}_2\text{O}_3$  powder, however, some agglomerates/bundles could be observed. No evidence of nanotubes damage after mixing can be observed. As seen in Fig. 1b, the unique flexible nature of SWCNTs makes them bend and pass through space between particles or wrap around them. Specific surface area of alumina powder and alumina/SWCNT composite powder are  $1.45 \text{ m}^2/\text{g}$  and  $5.16 \text{ m}^2/\text{g}$ , respectively. Figure 1c shows the particle size distribution of initial  $\text{Al}_2\text{O}_3$  powder. The sizes of alumina particles are distributed in the ranges of 97–409 nm, 453–842 nm, 933 nm–1.920  $\mu\text{m}$  and 2.129–9.992  $\mu\text{m}$ , which further confirms the observed result from SEM (Figure 1b) and the size with different ranges may be beneficial for dense packing of particles. The average particle size of alumina powder is  $1.71 \pm 0.45 \mu\text{m}$ .

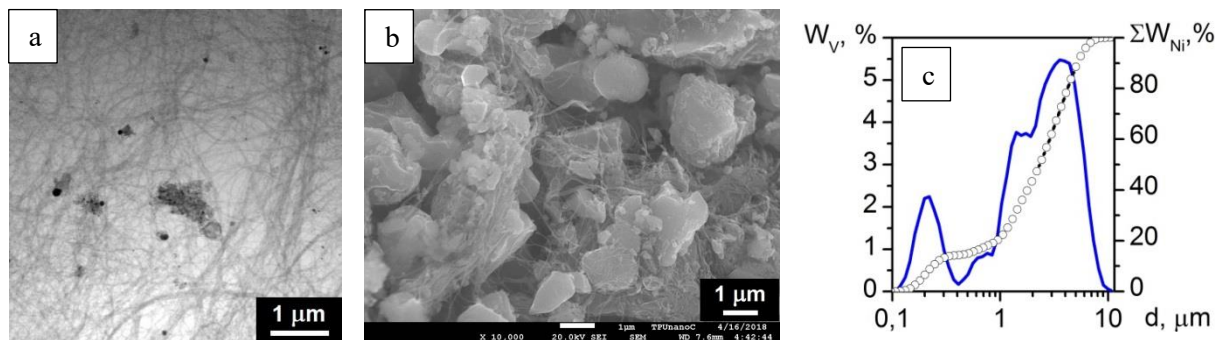


**Figure 1.** (a) TEM image showing morphology of SWCNTs, (b) SEM image showing morphology of composite powder and (c) particle size distribution of  $\text{Al}_2\text{O}_3$  powder.

After sintering by SPS, the produced materials were designated as A-1500, A-1600, AS-1500 and AS-1600 for samples of  $\text{Al}_2\text{O}_3$  ceramics sintered at 1500  $^\circ\text{C}$  and 1600  $^\circ\text{C}$  and  $\text{Al}_2\text{O}_3$ /SWCNT composites sintered at the same temperatures. The relative density, Vickers microhardness and fracture toughness are reported in Table 1. From Table 1 it can be seen that an increase in the sintering temperature of  $\text{Al}_2\text{O}_3$  ceramics to 1600  $^\circ\text{C}$  does not lead to an increase of the relative density; it is almost the same for both samples and was  $> 97\%$ . The relative density of composites ( $\sim 96\%$ ) was slightly lower than that of  $\text{Al}_2\text{O}_3$  ceramics, showing that SWCNTs inhibit the densification upon sintering, as observed in other studies [26–29]. The decrease in the sintered density upon the SWCNTs addition is due to the slightly reduced densification that leads to the increase of pores.

**Table 1.** Properties of the samples:  $\rho$ : relative density;  $H_V$ : Vickers microhardness and  $K_{IC}$ : fracture toughness (average, minimum/maximum values are indicated).

Sample	$\rho$ , %	$H_V$ (GPa)	$K_{IC}$ ( $\text{MPa}\cdot\text{m}^{1/2}$ )
A-1500	97.43	18.40 (16.94/19.70)	4.65 (4.00/5.16)
A-1600	97.20	17.64 (16.12/18.78)	4.34 (3.71/4.95)
AS-1500	95.91	16.58 (12.00/20.41)	4.94 (4.30/5.45)
AS-1600	96.10	16.60 (13.38/20.01)	3.95 (2.01/5.34)

The average microhardness of composites (16.60 GPa) is lower than that of  $\text{Al}_2\text{O}_3$  ceramics ( $\sim 18$  GPa) and has a higher scatter of values. The decrease in the microhardness by the addition of 3 vol% SWCNTs was attributed mainly to the decrease in the composite density. In addition, nanotubes are a soft phase. Although the hardness of SWCNTs was unknown, given that SWCNTs come from the graphitic family of carbon with dominantly  $\text{sp}^2$  bonds mixed with  $\text{sp}^3$  bonds, their hardness should be lower than that of  $\text{Al}_2\text{O}_3$ . Another factor is that the reinforcing phase usually creates tensile stresses in the crystals of the matrix and at their boundaries. Further, not very high sintering temperature also resulted in poor SWCNT/ $\text{Al}_2\text{O}_3$  interface that led to insufficient load sharing between filler and matrix in nanocomposites. However, it is worth noting that composites have high microhardness values (20.41 GPa and 20.01 GPa) that exceed the values of  $H_V$  for alumina

ceramics (Table 1). For a significant increase in the microhardness of composites with CNT required higher sintering temperature to achieve better consolidation and proper interface performance.

The fracture toughness of the AS-1500 composite is higher than that of samples A-1500 and A-1600 by 6 % and 12 %, respectively. The role of SWCNTs was indeed substantial, because the high strength, impressive flexibility and very high aspect ratio of the CNTs offered great potential for them to hold and resist the crack opening through elastic deformation. In this manner, SWCNTs worked efficiently for dissipating energy via transferring the stresses from one grain to another during the entire loading event, and for direct absorbing energy. Zharikov et al. [30] showed that alumina composite with 3 vol% CNTs have fracture toughness ( $6.6 \text{ MPa}\cdot\text{m}^{1/2}$ ) two times higher as compared to the initial ceramic material ( $3.2 \text{ MPa}\cdot\text{m}^{1/2}$ ). Kim et al. [31] have reached the maximum improvement in fracture toughness (about 40%,  $4.68 \text{ MPa}\cdot\text{m}^{1/2}$  vs  $3.32 \text{ MPa}\cdot\text{m}^{1/2}$ ) in 3 vol% CNTs/alumina composites. Zhang et al. [32] obtained the maximum increase in fracture toughness (24 %,  $4.1 \text{ MPa}\cdot\text{m}^{1/2}$  vs  $3.3 \text{ MPa}\cdot\text{m}^{1/2}$ ) by addition of 1 vol% CNTs. However, they reported only 6 % ( $3.5 \text{ MPa}\cdot\text{m}^{1/2}$ ) enhancement in fracture toughness for 3 vol% CNTs/ $\text{Al}_2\text{O}_3$  composites.

Figure 2 shows X-ray diffractograms and phase identification of powders SWCNTs (a),  $\text{Al}_2\text{O}_3$  (b) and sintered samples A-1500 and A-1600 (c, d), AS-1500 and AS-1600 (e, f). It can be seen that the phase composition of the  $\text{Al}_2\text{O}_3$  powder corresponds to the corundum ( $\alpha\text{-Al}_2\text{O}_3$ ) phase of the trigonal syngony (JCPDS No. 01-078-2426) [33], the CDD size of 48 nm (Figure 2b). Phase composition of the SWCNTs powder (Figure 2a) consists corresponds to graphite phase (JCPDS No. 01-075-1621) [33, 34], the CDD size of 8 nm. The existence of (110) lattice planes indicates a developed in-planar graphitic structure and (101) planes can be considered to be to the foreign of three-dimensional stacking, mainly caused by the lack of defects in the SWCNT [34]. In addition, SWCNTs powder contains catalyst residues corresponding to the bcc structure, in the apparent, of Fe (JCPDS No. 01-085-1410) with a lattice parameter of  $2.88686\cdot 10^{-10}$  and  $\text{Fe}_3\text{C}$  (JCPDS No. 35-0772).

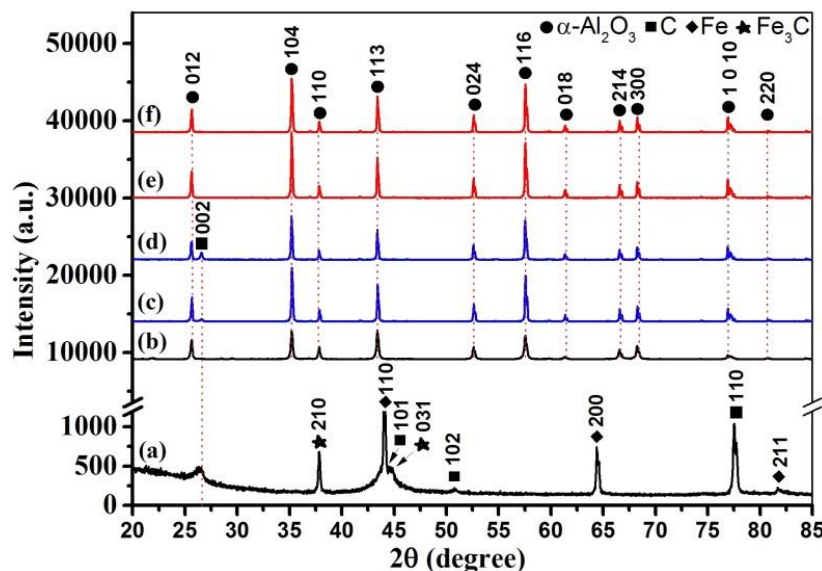


**Figure 2.** X-ray diffractograms and phase identification of powders SWCNTs (a),  $\text{Al}_2\text{O}_3$  (b) and sintered samples A-1500 and A-1600 (c, d), AS-1500 and AS-1600 (e, f).

After sintering of  $\text{Al}_2\text{O}_3$  powder (A-1500 and A-1600), a two-phase state is formed with the creation of a second carbon-like structure, the integral intensity of which is 7 % and 19 %, respectively (Figure 2c, d). Apparently, this may be due to the contamination of the powder during the granulation of  $\text{Al}_2\text{O}_3$  or with graphite paper residue after SPS sintering. The CDD size of the main phase  $\alpha\text{-Al}_2\text{O}_3$  is 81 nm (A-1500) and 80 nm (A-1600), the second carbon-containing phase is 33 nm (A-1500) and 41 nm (A-1600). Only peaks corresponding to crystalline  $\alpha\text{-Al}_2\text{O}_3$  were in the diffractograms of the

AS-1500 and AS-1600, whereas CNT peaks were absent (Figure 2e, f). Owing to small quantity of SWCNTs in the composites (3 vol%) and strong matrix peaks, identification of  $sp^2$  carbon phase was not possible [35-37]. The CDD size of  $\alpha$ - $Al_2O_3$  with increasing sintering temperature was constant and amounted to 82 nm.

#### 4. Conclusions

The effect of SWCNTs on sintering behavior and mechanical properties behavior of  $Al_2O_3$ /SWCNTs composites obtained by spark plasma sintering was investigated. The following conclusions can be drawn from this study:

- Sintered densities  $\sim 96$  % of theoretical density were obtained in the composites.
- The average microhardness of the composites was lower than that of  $Al_2O_3$  ceramics, but there were also high microhardness values of composites (20.41 GPa).
- The fracture toughness ( $4.94 \text{ MPa} \cdot \text{m}^{1/2}$ ) of the AS-1500 composite was higher than that of  $Al_2O_3$  ceramics samples A-1500 and A-1600 by 6 % and 12 %, respectively.
- The phase composition of the composites corresponds to the crystalline  $\alpha$ - $Al_2O_3$ , SWCNT peaks were absent. The CDD size of  $\alpha$ - $Al_2O_3$  with increasing sintering temperature was constant and amounted to 82 nm.

#### References

- [1] Osayande L and Okoli O I 2008 Fracture toughness enhancement for alumina system: a review *Int. J. App. Ceram. Technol.* **5** 313–323
- [2] Krenkel W 2008 *Ceramic Matrix Composites: Fiber Reinforced Ceramics and their Applications* (Weinheim: Wiley-VCH Verlag GmbH & Co.KGaA) p 443
- [3] Chawla K K 2012 *Composite Materials: Science and Engineering* (New York: Springer-Verlag)
- [4] Estili M and Sakka Y 2014 Recent advances in understanding there inforcing ability and mechanism of carbon nanotubes in ceramic matrix composites *Sci. Technol. Adv. Mater.* **15** 064902
- [5] Hussainova I, et al. 2016 Wear performance of hierarchically structured alumina reinforced by hybrid graphene encapsulated alumina nanofibers *Wear* **368–369** 287–295
- [6] Dudkin B N, et al. 2010 Corundum/lanthanum hexaaluminate/alumina nanofiber ceramic composite *Inorg. Mater.* **46** 445–448
- [7] Tamura Y, et al. 2017 Spark plasma sintering of fine-grained alumina ceramics reinforced with alumina whiskers *Ceram. Int.* **43** 658–663
- [8] Tamura Y, et al. 2018 Is an alumina-whisker-reinforced alumina composite the most efficient choice for an oxidation-resistant high-temperature ceramic? *J. Eur. Ceram. Soc.* **38** 1812–18
- [9] Robertson T, et al. 2016 High temperature performance of mullite whisker-reinforced ZTA *J. Compos. Mater.* **50(26)** 3719–29
- [10] Lu Z L, et al. 2016 Effect of in situ synthesised mullite whiskers on the high-temperature strength of  $Al_2O_3$ -based ceramic moulds for casting hollow turbine blades *Ceram. Int.* **42** 18851–58
- [11] Wu W, et al. 2017 The effect of residual stress on whisker reinforcements in  $SiC_w$ - $Al_2O_3$  composites during cooling *J. Alloy. Compd.* **725** 639–643
- [12] Lee D Y and Yoon D H 2014 Properties of alumina matrix composites reinforced with SiC whisker and carbon nanotubes *Ceram. Int.* **40** 14375–83
- [13] He P, et al. 2016 Preparation and mechanical performance of ductile  $C_{sf}/Al_2O_3$ -BN composites, Part 1: effects of fiber length and sintering temperature *Ceram. Int.* **42** 9821–29
- [14] Jia J, et al. 2018 Preparation and mechanical properties of short carbon fibers reinforced  $\alpha$ - $Al_2O_3$ -based composites *Ceram. Int.* **44** 19345–51
- [15] Castillo-Rodríguez M, et al. 2018 Creep study on alumina and alumina/SWCNT nanocomposites *J. Eur. Ceram. Soc.* **38** 5497–02
- [16] Leonov A A, et al. 2017 Spark plasma sintering of ceramic matrix composite based on alumina,

- reinforced by carbon nanotubes *IOP Conf. Ser.: Mater. Sci. Eng.* **286** 012034
- [17] Asiq Rahman O S, et al. 2018 Synergistic effect of hybrid carbon nanotube and graphene nanoplatelets reinforcement on processing, microstructure, interfacial stress and mechanical properties of  $\text{Al}_2\text{O}_3$  nanocomposites *Ceram. Int.* **44** 2109–22
- [18] Golovin Y I, et al. 2018 Effect of carbon nanotubes on strength characteristics of nanostructured ceramic composites for biomedicine *Nanotechnol Russia* **13** 168–172
- [19] Wang W L, et al. 2011 Fabrication of alumina ceramic reinforced with boron nitride nanotubes with improved mechanical properties *J. Am. Ceram. Soc.* **94** 3636–40
- [20] Wang W L, et al. 2011 Microstructure and mechanical properties of alumina ceramics reinforced by boron nitride nanotubes *J. Eur. Ceram. Soc.* **31** 2277–84
- [21] Zhan G D, et al. 2003 Single-wall carbon nanotubes as attractive toughening agents in alumina-based nanocomposites *Nat. Mater.* **2** 38–42
- [22] Bi S, Hou G, Su X, et al. 2011. Mechanical properties and oxidation resistance of  $\alpha$ -alumina/multi-walled carbon nanotube composite ceramics *Mater. Sci. Eng. A* **528** 1596–1601
- [23] Bocanegra-Bernal M H, et al. 2017 Effect of low-content of carbon nanotubes on the fracture toughness and hardness of carbon nanotube reinforced alumina prepared by sinter, HIP and sinter + HIP routes *Mater. Res. Express* **4** 085004
- [24] Anstis G R, et al. 1981 A critical evaluation of indentation techniques for measuring fracture toughness: I, direct crack measurements *J. Am. Ceram. Soc.* **64** 533–538
- [25] Peigney A, et al. 2001 Specific surface area of carbon nanotubes and bundles of carbon nanotubes *Carbon* **39** 507–514
- [26] Ahmad I, et al. 2018 Synergic influence of MWCNTs and SiC nanoparticles on the microstructure and properties of  $\text{Al}_2\text{O}_3$  ceramic hybrid nanocomposites *Curr. Appl. Phys.* **16** 1649–58
- [27] Hanzel O, et al. 2017 Mechanical and tribological properties of alumina-MWCNTs composites sintered by rapid hot-pressing *J. Eur. Ceram. Soc.* **37** 4821–31
- [28] Aguilar-Elguézabal A and Bocanegra-Bernal M H 2014 Fracture behaviour of  $\alpha$ - $\text{Al}_2\text{O}_3$  ceramics reinforced with a mixture of single-wall and multi-wall carbon nanotubes *Compos. Part B* **60** 463–470
- [29] Ghobadi H, et al. 2014 Improving CNT distribution and mechanical properties of MWCNT reinforced alumina matrix *Mater. Sci. Eng. A* **617** 110–114
- [30] Zharikov E V, et al. 2016 Reinforcement of  $\text{Al}_2\text{O}_3$ -MgO composite materials by multiwalled carbon nanotubes *Inorg. Mater. Appl. Res.* **7** 163–169
- [31] Kim S W, et al. 2009 Improvement of flexure strength and fracture toughness in alumina matrix composites reinforced with carbon nanotubes *Mater. Sci. Eng. A* **517** 293–299
- [32] Zhang S C, et al. 2010 Pressureless sintering of carbon nanotube- $\text{Al}_2\text{O}_3$  composites *J. Eur. Ceram. Soc.* **30** 1373–80
- [33] Ahmad I, et al. 2010 Carbon nanotube toughened aluminium oxide nanocomposite *J. Eur. Ceram. Soc.* **30** 865–873
- [34] Estili M, et al. 2008 The homogeneous dispersion of surfactantless, slightly disordered, crystalline, multiwalled carbon nanotubes in  $\alpha$ -alumina ceramics for structural reinforcement *Acta Mater.* **56** 4070–79
- [35] Shahzad H K, et al. 2018 Synthesis and characterization of alumina-CNT membrane for cadmium removal from aqueous solution *Ceram. Int.* **44** 17189–98
- [36] Shin J H, et al. 2018 Comparative study on carbon nanotube- and reduced graphene oxide-reinforced alumina ceramic composites *Ceram. Int.* **44** 8350–57
- [37] Sikder P, et al. 2015 Indentation size effect and wear characteristics of spark plasma sintered, hard MWCNT/ $\text{Al}_2\text{O}_3$  nanocomposites *Adv. Appl. Ceram.* **114** 448–455